Optical Engineering 49(11), 111114 (November 2010)

Nonlinear coupling of transverse modes in quantum cascade lasers

Aleksander K. Wójcik
Texas A&M University
Department of Physics and Astronomy
College Station, Texas 77843

Nanfang Yu
Laurent Diehl
Federico Capasso
Harvard University
School of Engineering and Applied Sciences
Cambridge, Massachusetts 02138

Alexey Belyanin
Texas A&M University
Department of Physics and Astronomy
College Station, Texas 77843
E-mail: belyanin@tamu.edu

Abstract. We study the multimode operation regimes of midinfrared quantum cascade lasers (QCLs), taking into account nonlinear phase-sensitive interactions between transverse modes. We show the possibility of the coherent coupling of several transverse modes, which results in a number of interesting effects including frequency and phase locking between transverse modes, bistability, and beam steering. We present an analytical model for the modal dynamics and its numerical analysis. Effects of amplitude and phase fluctuations on the modal stability are explored. The theoretical results are in agreement with our experimental measurements of buried heterostructure QCLs. © *2010 Society of Photo-Optical Instrumentation Engineers*. [DOI: 10.1117/1.3498773]

Subject terms: nonlinear optics; quantum cascade lasers; phase coherence; mode locking.

Paper 100314SSR received Apr. 11, 2010; revised manuscript received Jul. 9, 2010; accepted for publication Jul. 12, 2010; published online Nov. 30, 2010.

1 Introduction

Nonlinear interaction of mid/far-infrared radiation with the active region in quantum cascade lasers (QCLs) is extremely strong due to a large matrix element of the optical transitions between delocalized electron states in coupled quantum wells. Even more importantly, the active region of a QCL can be modified to enhance any particular nonlinear optical interaction by adjusting intersubband resonances and oscillator strengths. This greatly facilitates intracavity frequency conversion processes such as generation of harmonics,[1–3] difference frequency in the terahertz range,[4,5] and stimulated Raman scattering.[6]

At the same time, the nonlinear coupling between laser cavity modes within the gain spectrum of the laser transition, which is so prominent in other types of solid-state lasers and which leads to a variety of mode-locking phenomena, is suppressed in QCLs by ultrafast gain recovery time of the order of 1 ps. This timescale is much shorter than the cavity roundtrip time and the photon lifetime (a class A laser[7]). This leads to a strong damping of any perturbation of light intensity in a cavity, except maybe in the fully coherent regime when the timescale of Rabi oscillations of the population inversion and laser intensity becomes shorter than the dephasing time of the optical polarization (see Refs. 8, 9, and 10). Although in recent work,[11] active mode locking by gain modulation in a short section of a QCL cavity has been demonstrated near laser threshold, passive mode locking remains an elusive goal. Surprisingly, in a recent study[12] we found out that the phases of different *transverse* modes can be coupled in a standard QCL without a saturable absorber or any other nonlinear element in a cavity. The coherence of mutual phases of three or four transverse modes has been verified by near- and far-field measurements, observation of the beam steering effect, and theoretical modeling, which predicted modal amplitudes, frequencies, and phases in agreement with the experiment.[12] In the present work, we report systematic studies of multilateral mode QCLs, which indicate that nonlinear locking of lateral modes is a ubiquitous phenomenon for buried-heterostructure lasers. We describe a recently found regime of complete synchronization when combs of longitudinal modes belonging to different lateral modes merge into a single comb; see the second reference in Ref. 12.

2 Experimental Evidence for Transverse Mode Locking

Higher order lateral modes are routinely observed in QCLs with waveguide widths exceeding three to four laser wavelengths in a medium. For example, in the recent study of broad-area ridge-waveguide QCLs,[13] a variety of multilateral mode operation regimes were readily observed, although no evidence for the nonlinear mode coupling was found. However, the transverse modes do interact with each other through the inhomogeneous saturation of the active region (spatial hole burning effect). In certain cases, this nonlinear interaction can prevail over the waveguide dispersion and result in phase and frequency locking.

Coherent transverse effects in lasers have been the subject of extensive research over several decades. Dynamical transverse laser pattern formation has been studied in the context of laser instabilities,[14,15] structured light,[16] transverse pattern formation and control,[17,18] and solitons.[19] For a review of the work dating prior to the nineties, see Abraham and Firth and references therein.[20] Limited work on the subject has been done on QCLs. One possible signature of the transverse mode coherence in QCLs is the asymmetry in the near and far field of a laser beam, observed, for example, in Refs. 12, 21, and 22. QCLs operating in the mid-infrared range have the advantage of having a longer wavelength, which allows the fabrication of subwavelength metallic or dielectric patterns on the laser cavity, resulting in radiation

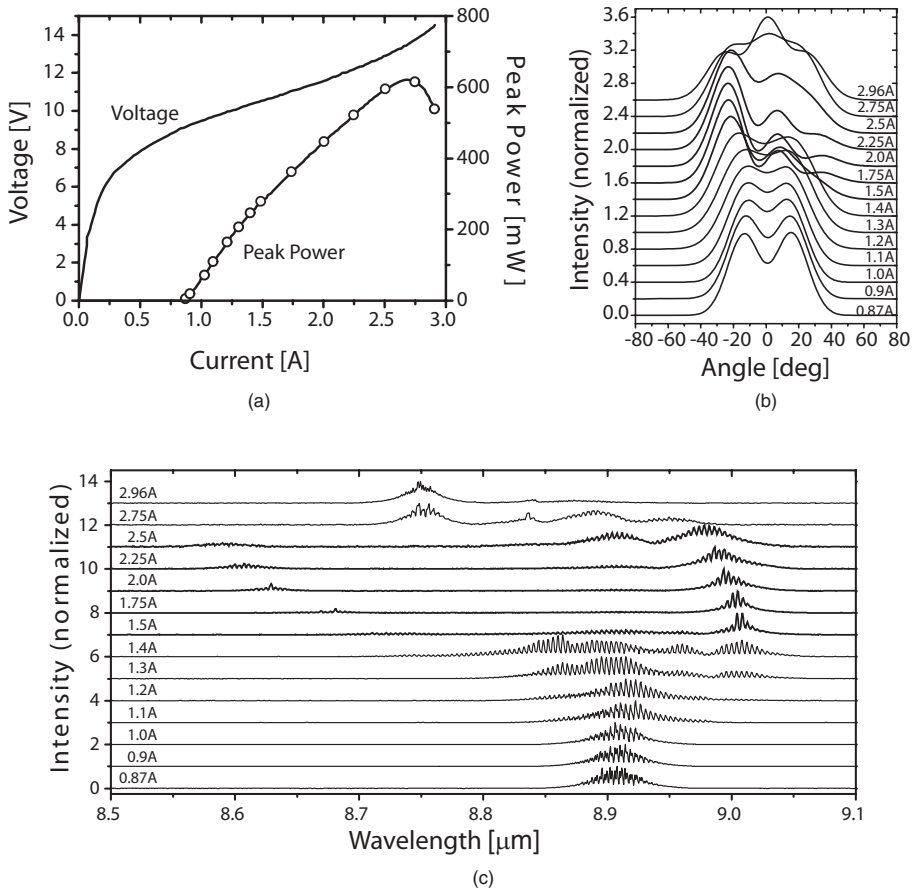

Fig. 1 (a) Measured LIV curve, (b) the far field, and (c) the spectra of a buried-heterostructure QCL with wavelength $\lambda \approx 8.9$ μm and an active region 19.4 μm wide, fabricated by Hamamatsu.

pattern control and plasmonic beam shaping (see, e.g., Ref. 23 for the review). This combined with multitransverse mode operation can result in dynamic light structures and selective transverse mode control.

In recent work,[12] we have shown that the observed axial asymmetry and beam steering of the radiated field in QCLs can be a manifestation of phase coherence between several lateral modes. Phase locking between lateral modes can be explained through four-wave mixing utilizing resonant third-order $[\chi^{(3)}]$ optical nonlinearity in the active region originated from inhomogeneous gain saturation. The processes that affect nonlinear mode coupling in QCLs differ considerably from those in diode lasers, where multitransverse mode behavior has been previously observed and analyzed.[24] As we already pointed out, QCLs should demonstrate class-A laser behavior,[7] accompanied by weak carrier diffusion and strong hole burning effects, as opposed to diode lasers that show class-B dynamics, strong carrier diffusion, and weak spectral and spatial hole burning.

Although thermal effects can lead to a temperature-dependent refractive index and far-field distortion in QCLs,[22] these effects do not lead to sudden changes in the spectra, frequency locking, and modal phase coherence. Our experimental results, near- and far-field fitting, and Fourier analysis of the laser spectra confirmed the presence of these phenomena in the analyzed lasers. The observed coherent coupling of the transverse modes can only be explained by their nonlinear interaction.

Even though the phases of the transverse modes observed in Ref. 12 were correlated, their combs remained distinct and there was no sudden change in the spectra at the onset of phase locking. Here we describe an even more fascinating effect of the complete mode synchronization, in which a complex spectrum of several distinct combs of longitudinal modes belonging to different transverse modes merges into a single comb while the laser maintains a multi-transverse mode operation; see the second reference in Ref. 12. The transition to this regime occurs as a bifurcation at a certain value of the injection current. It is accompanied by the transition from the multistability regime, where many stable steady-state solutions are possible to the regime where there exists only one stable steady state with phase coherence between lateral modes.

An experimental example of such frequency- and phase-locked behavior is presented in Fig. 1, which corresponds to a buried-heterostructure laser fabricated by Hamamatsu (Japan), with an active region width of 19.4 μm. This is a high-performance laser based on a three-phonon resonance design as reported in Refs. 11 and 25. It is operated in a pulsed-mode, 125-ns pulse length, 1% duty cycle at room temperature. Starting from threshold, this laser shows three lateral modes of TM_{00}, TM_{01}, and TM_{02}, and its far field is well described by an incoherent addition of modal intensities. The spectrum consists of at least three distinct combs of longitudinal modes, each comb belonging to a different lateral mode. At about 1.5 A, both the spectrum and the far

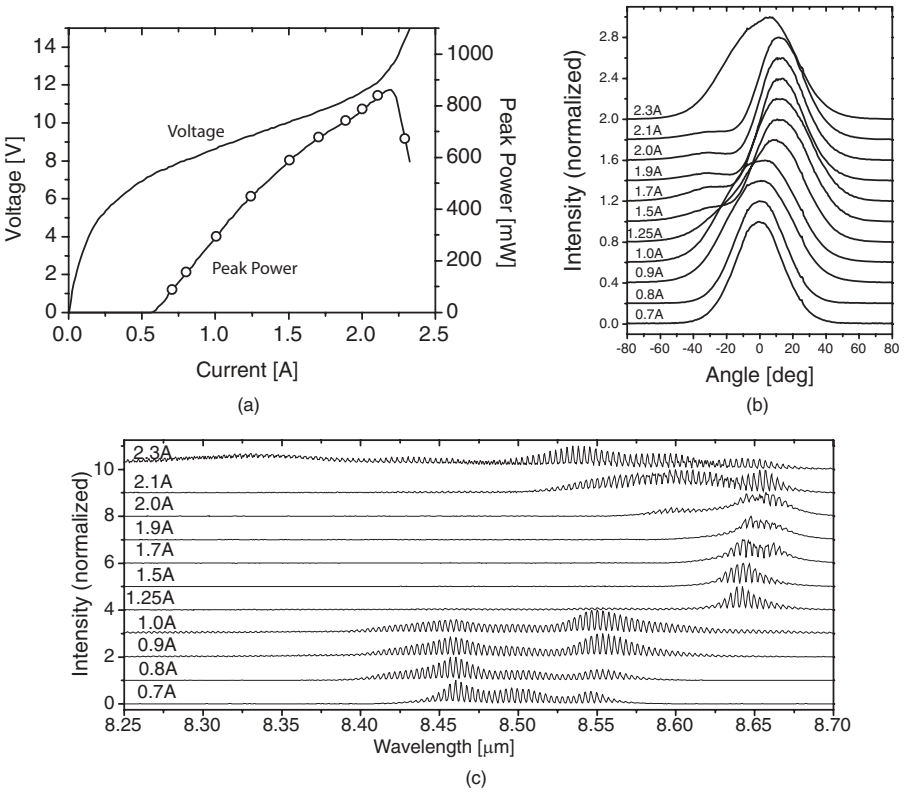

Fig. 2 (a) Measured LIV curve, (b) the far field, and (c) the spectra of a buried-heterostructure QCL with wavelength $\lambda \approx 8.45\ \mu$m and an active region 11.2 μm wide, fabricated by Agilent.

field undergo a drastic change. The spectral combs merge into a single comb [Fig. 1(c)], as if only one lateral mode is present. This locking of lateral modes is verified by Fourier analysis of the spectra below and above the bifurcation value of the current. This analysis reveals three distinct rf peaks below the locking transition, which correspond to the roundtrip frequencies in three combs. Only one such peak exists above the locking transition. At the same time, the far-field pattern becomes very asymmetric and shifts by about 30 deg off the waveguide axis [Fig. 1(b)]. This far field indicates the presence of all three lateral modes whose combs become completely synchronized. Moreover, we verified that the far field can only be fitted by a *coherent* addition of the fields of all three lateral modes with fixed mutual phases. Any incoherent addition of mode intensities cannot lead to the observed asymmetric distribution, because all lateral modes are symmetric with respect to the waveguide axis.

This frequency-synchronized, phase-coherent behavior persists over a wide range of currents and is reproducible. Then at about 2.75 A, the laser undergoes transition back to a state with several distinct spectral combs and symmetric far-field patterns.

Another buried heterostructure laser (from Agilent, Santa Clara, California) showing similar behavior is shown in Fig. 2. This is a metal organic chemical vapor deposition (MOCVD)-grown laser based on a double phonon resonance design of the active region.[26] It lases at a wavelength $\lambda \approx 8.45\ \mu$m and the waveguide is 11.2 μm wide. The light-current-voltage (LIV) curve, far-field measurements, and spectra are presented in Fig. 2. The laser is operated in the same regime as the Hamamatsu devices: at room temperature in a pulsed regime, with 125-ns pulses. The experimental conditions and setup are the same as the ones described in Ref. 12.

The laser beam shows asymmetry for currents between 1.25 and 2.1 A. Above this current, the laser enters into a rollover region. The beam steering region of currents correlates with the change in the laser spectrum and is accompanied by frequency and phase locking, although the combs remain distinct in this case, as revealed by the Fourier analysis and far-field fitting, similar to the case studied in Ref. 12.

We emphasize that the existence of this phase-locked regime within a certain range of currents is not a unique property of one peculiar laser device. In total, four Hamamatsu lasers and 11 Agilent lasers with different waveguide widths have been tested. All of them show anomalous (asymmetric) far-field patterns with different degrees of asymmetry, accompanied by strong changes in the laser spectra. About one third of them show the frequency locking effects; the rest do not show the locking of modal combs, likely due to incomplete lateral mode locking. The common property between different devices was that all devices were of buried-heterostructure type, with the active stripe overgrown by a thick low-loss dielectric cladding. This design gives rise to very similar losses for several lateral modes. In fact, most of the devices started lasing at a higher order lateral mode. In comparison, in the recent study of broad-ridge QCLs with lossy metal sidewalls,[13] multilateral mode operation was readily observed, but no indication of phase coherence was found. A probable reason for this is a much larger losses for high order lateral modes in the ridge waveguide as compared to buried-heterostructure devices. Our numerical analysis does show that in this situation the transverse mode locking would be suppressed.

3 Theoretical Model

We consider the simplest possible model for the dynamics of the transverse modes in QCLs, which still includes the effect of phase-sensitive nonlinear mode coupling. The material gain is modeled as a two-level medium, resulting in Maxwell-Bloch equations. The polarization and population variables are eliminated adiabatically (class-A laser), resulting in a system of nonlinear differential equations for complex amplitudes of cavity modes, to which amplitude and phase fluctuations are added phenomenologically. The equations are solved numerically in the time domain, and the dynamics of the modes are systematically studied as a function of laser parameters: gain, losses, frequency detunings, etc. Our analysis is compared with experimental results for buried-heterostructure QCLs. The results can be used to understand and control the effects of phase locking, beam steering, and pulsed operation in the midinfrared range.

3.1 *Equations of Motion*

Our analysis starts with a set of two-level Maxwell-Bloch equations, in which we perform modal decomposition of the electric field into waveguide modes, and the adiabatic elimination of the population inversion and coherence. The final derivation leads to a system of coupled nonlinear equations for complex amplitudes of the cavity modes.

Starting with Maxwell's equations, we decompose the electric field in the cavity into a sum of quasiorthogonal waveguide modes:

$$\mathbf{E} = \sum_i e_i(t,z)\mathbf{E}_i(\mathbf{r}_\perp), \tag{1}$$

where $\boldsymbol{r}_\perp$ is the radius vector in the cross section of the waveguide and z is the coordinate along the cavity. We introduce slowly varying complex amplitudes of the electric field:

$$e_i = \tfrac{1}{2}[a_i \exp(-i\omega_0 t + i\beta_i z) + a_i^* \exp(i\omega_0 t - i\beta_i z)], \tag{2}$$

where ω_0 is the laser transition frequency and β_i is the propagation constant of the i'th mode.

The active region is modeled using density matrix equations for a two-level medium, with optical polarization expressed through a slowly varying amplitude σ of the off-diagonal element of the density matrix as

$$P = Nd[\sigma \exp(-i\omega_0 t) + \sigma^* \exp(i\omega_0 t)]. \tag{3}$$

By integrating Maxwell's equations over the cross section A_T of the waveguide, making use of the orthogonality of the modes, and eliminating the fast oscillating terms (rotating wave approximation), we obtain

$$\frac{\partial\sigma}{\partial t} + \gamma_\perp\sigma = -\frac{id}{2\hbar}D\sum_i E_i a_i, \tag{4}$$

$$\frac{\partial D}{\partial t} + \gamma_\parallel(D - D_p) = -\frac{id}{\hbar}\sum_i (a_i^*\sigma - a_i\sigma^*), \tag{5}$$

$$\frac{\partial a_i}{\partial t} + \frac{c}{\mu_i}\frac{\partial a_i}{\partial z} + (\kappa_i + i\Delta_{ci})a_i = \frac{4\pi i\omega_0 Nd}{\mu_i A_T}\int_{AR}\sigma E_i dA, \tag{6}$$

where N is the total electron density in the active region, d is the dipole moment of the laser transition, Δ_{ci} is the detuning of the i'th mode from the central frequency ω_0, μ_i is the modal refractive index, $\gamma_\perp^{-1}$ and $\gamma_\parallel^{-1}$ are relaxation times for coherence and population inversion, respectively, and D_p is the population inversion supported by pumping in the absence of laser generation.

In the present section, under the mean-field approximation, the detuning variables represent the separation between adjacent transverse modes. In the second part of this work, we analyze the case where a given number of longitudinal modes is analyzed (five per each lateral modes) and their detunings are determined by the cavity modal structure.

The relaxation times in QCLs are faster than photon decay times, which allows us to perform adiabatic elimination of the polarization $d\sigma/dt = 0$ and population $dD/dt = 0$. We expand the polarization term in series and retain only the first two terms [$\chi^{(3)}$ approximation]. Since we have a large number of longitudinal modes per one lateral mode, as seen in the experimental spectra next, we employ the mean-field approximation by averaging the last equation over z and including mirror losses into the total losses κ_i. The equation of motion for the i'th mode becomes as follows:

$$\frac{da_i}{dt} + (\kappa_i + i\Delta_{ci})a_i = g\Gamma_i a_i - \frac{g}{I_S}\sum_{j,k,l} a_j a_k^* a_l G_{ijkl}, \tag{7}$$

where the material gain and saturation intensity are defined by

$$g = \frac{2\pi\omega_0 N d^2 D_p}{\gamma_\perp\hbar\mu_i}, \quad I_S = \frac{\hbar^2\gamma_\parallel\gamma_\perp}{d^2}. \tag{8}$$

Here the overlap integrals are defined as

$$\Gamma_i = \frac{\int_{AR}\varepsilon E_i^2 dA}{\int_{A_T}\varepsilon E_i^2 dA}, \quad O_i = \frac{1}{A_T}\int_{AR}\varepsilon E_i^2 dA, \tag{9}$$

$$G_{ijkl} = \frac{1}{A_T(O_i O_j O_k O_l)^{\frac{1}{2}}}\int_{AR}\varepsilon E_i E_j E_k E_l dA, \tag{10}$$

where AR is the cross sectional area of the active region. The factors G_{ijkl} are symmetric with respect to any permutation of the subindices, which is clear from the definition in Eq. (10). The symmetry simplifies the numerical calculations.

The second term on the right-hand side of Eq. (7) describes the phase-sensitive nonlinear coupling between different modes, which can lead to their frequency and phase locking. This process competes with the effect of waveguide dispersion and losses described by the complex detunings [the second term on the left-hand side of Eq. (7)].

As the final step, we add phenomenologically a noise term to the equations. Since the QCLs are class-A lasers, noise analysis differs from that of standard semiconductor lasers, and it gets more complicated by the correlation of photons through the reuse of electrons while they travel inside the cavity. The specifics of noise correlation effects are discussed in the literature.[27,28]

Our numerical analysis showed that fluctuations in the injection current do not influence the basic behavior of the modes, and we neglect it to concentrate on fluctuations of the complex amplitudes of the modes. One possible source of these fluctuations is the spontaneous emission.

The noise enters our equations as an extra equation, with a stochastic source term added to the complex field amplitude,

$$a_i(t) \to a_i(t) + \tilde{a}\xi_i(t). \tag{11}$$

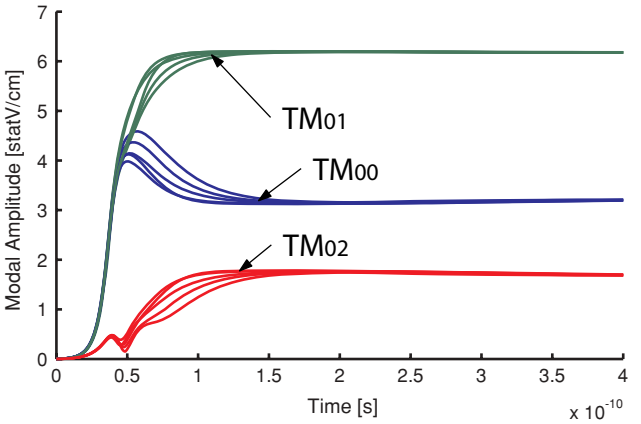

Fig. 3 Time-dependent dynamics of modal amplitudes for five random initial conditions. The gain is 3.5 times g_{th}.

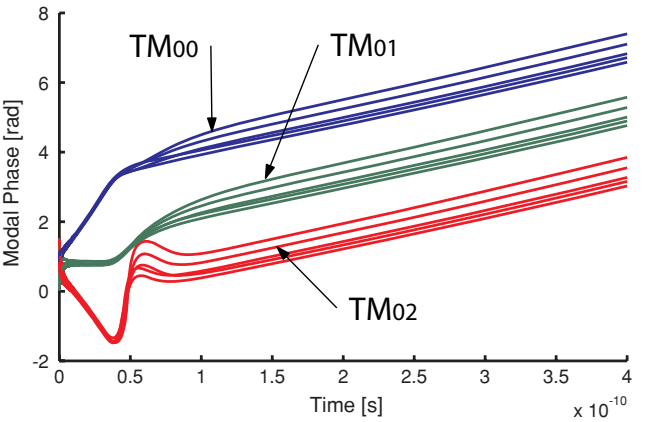

Fig. 4 Phases corresponding to the same simulations as in Fig. 3.

The noise term has the following characteristics:

$$\langle \xi_i(t) \rangle = 0,$$

$$|\langle \xi_i(t)\xi_j(t') \rangle| = \delta_{ij}\delta(t-t'). \tag{12}$$

Here $\tilde{a}$ is the noise amplitude and $\xi(t)$ is a stochastic process, with a complex uniform distribution function and $0 \leq |\xi(t)| \leq 1$.

3.2 *Numerical Modeling*

We solve the resulting system of coupled nonlinear differential equations [Eq. (7)] numerically. The initial conditions for the amplitudes are taken as a set of randomly distributed complex amplitudes, with magnitudes of the order of 10^{-3}. This accounts for the amplification of the cold cavity modes from spontaneous emission. The equations are integrated until the amplitudes reach either steady state or a periodic form. In the present section, we focus on three transverse modes, which is the number of modes observed in our experiments.

An example of the dynamics of three transverse modes is presented on Fig. 3. The modes are the TM_{00}, TM_{01}, and TM_{02} modes. The transverse distributions, losses, frequencies, and propagation constants of cold waveguide modes were found with COMSOL software using the finite element method, and were consequently used to find the overlap integrals G and Γ. The laser geometry corresponded to buried-heterostructure lasers, shown in the experimental section next. Details of the mode calculation methodology can be found in Ref. 29. The values of parameters used for the simulations are presented in Table 1. The gain g_{th} is the threshold gain for the TM_{01} mode, which has the lowest threshold.

Table 1 Parameters and modes used in the simulations.

Mode	TM_{00}	TM_{01}	TM_{02}
Δ_{ci} (rad/s)	-6.52×10^{10}	0	6.29×10^{10}
κ_i (rad/s)	7.86×10^{10}	6.82×10^{10}	9.08×10^{10}
Γ	0.517	0.496	0.448
I_S (erg/s/cm^2)		1.21×10^{3}	
$\tilde{a}$ (statV/cm)		1×10^{-2}	
g_{th} (rad/s)		1.37×10^{11}	

Next, we find stable-steady state solutions by solving Eq. (7) starting from a large set of random initial conditions and following the modal evolution with time until a stable solution is reached. An example of such analysis is shown in Fig. 3 for the amplitudes and Fig. 4 for the phases of complex amplitudes a_i. The nonlinear interaction leads to frequency pulling, merging the transverse modes into a single frequency with a constant phase difference between them. This can be observed from Fig. 4 as well, where the slope of the phase is the frequency. Experimentally, this effect should lead to merging of three combs belonging to different transverse modes into a single comb, while the far-field pattern shows the presence of all three transverse modes with locked phases. The phase difference between the modes determines the exact form and amount of beam steering in the far field.

The same time-dependent simulations starting from a random set of initial conditions were made for a broad range of gain values. The values of the parameters were the same as before, only the parameter g was varied. The results are plotted in Figs. 5 and 6, where the gain is normalized to the value g_{th} from Table 1.

The three modes lock to a single frequency, forming a gain-dependent far-field pattern. The dominant mode TM_{01} starts lasing with a normalized gain of 1, while the other

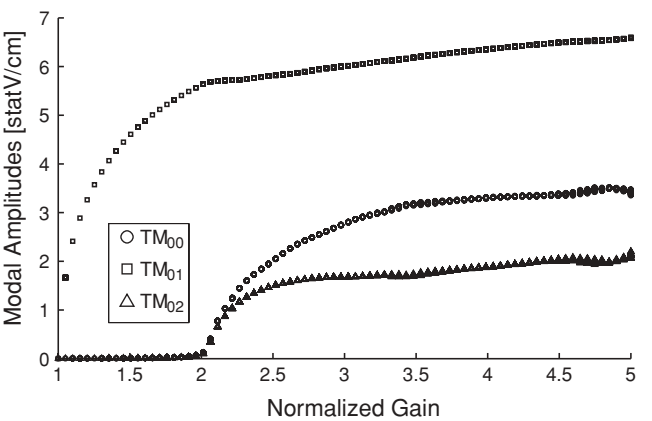

Fig. 5 Amplitudes of the modes as a function of gain, normalized to g_{th}. All three modes are present.

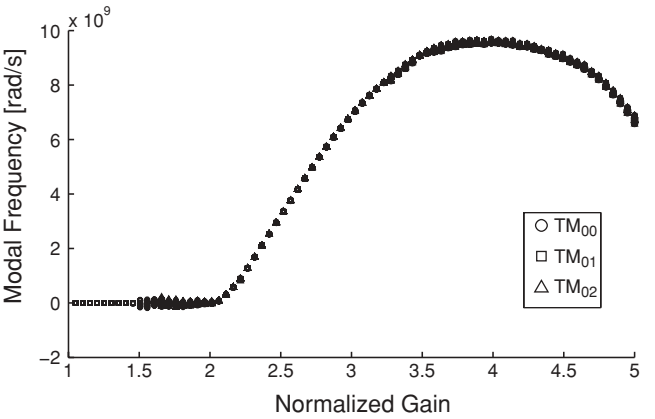

Fig. 6 Frequencies of the modes as a function of gain, normalized to g_{th}. The modes lock to a single frequency.

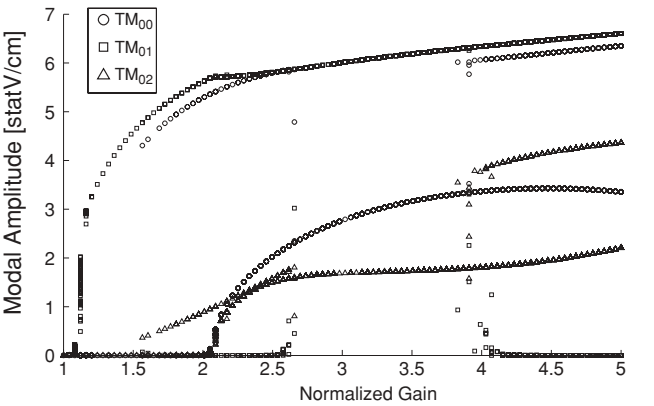

Fig. 8 Bistability in modal amplitudes as a function of gain, normalized to g_{th}.

two modes appear almost simultaneously when the gain is two times higher, as seen from Fig. 6. The relative phase of the modes also depends of the gain, varying almost monotonously, as presented in Fig. 7. The figure shows only the phase relation between modes TM_{00} and TM_{02} at the final time of the simulation. This phase dependence of the gain determines the exact angular distribution of the pump-dependent asymmetric beam pattern.

We extend our analysis to the case where noise becomes negligible, which in our case represents taking the noise amplitude $\tilde{a}$ below approximately 1×10^{-3} statV/cm. In this case, the laser shows bistability behavior. The amplitudes of steady-state solutions from a time-dependent simulation are shown in Fig. 8. The simulation is repeated for the same value of gain, but randomly taking another set of initial conditions. The final amplitude takes one of the two branches depending of the initial condition – the effect that did not exist when the noise was an order of magnitude higher. All transverse modes lock to the same frequency, but this frequency is different for each of the bistable states, as shown in Fig. 9.

Interestingly, there exists an intermediate range of gains where only one stable steady-state solution exists, as shown in Figs. 8 and 9. The two boundaries of this region are points of bifurcations where the second solution appears. In the immediate vicinity of each boundary, there is an unstable region where multiple solutions exist, depending on the initial conditions and the level of noise. In this region the laser is expected to randomly hop between different mode patterns.

The coexistence of two stable solutions may seem puzzling, but close inspection of Fig. 8 reveals that the second stable solution contains only two lateral modes – the third mode has zero amplitude. The latter mode is actually the TM_{01} mode, which has the lowest threshold and starts lasing first when the pump is turned on; therefore, its suppression and the emergence of the second, two-mode solution is entirely due to a strong nonlinear interaction and competition between modes.

The bistability effect is not strongly dependent of the spectral separation between the cold waveguide modes, or Δ parameters in our model. We explored the dependence of the modal amplitude on a Δ plane, and observed that bistability is fairly independent of Δ_3 and needs a certain threshold for $\Delta_{1,th} < \Delta_1$ to appear, as can be seen from Figs. 10 and 11. In the case analyzed here, $\Delta_{1,th} \simeq 0.05$ meV, which is about half the frequency separation between neighboring longitudinal modes within one comb.

The amplitude of the mode TM_{00} is different from 0, independently of Δ_3 as long as Δ_1 is below 0.05 meV. The same case follows for mode TM_{02}, as long as Δ_3 is below 0.05 meV. The separation of the modes depends directly on the shape of the cavity and the design of the QCLs. A more

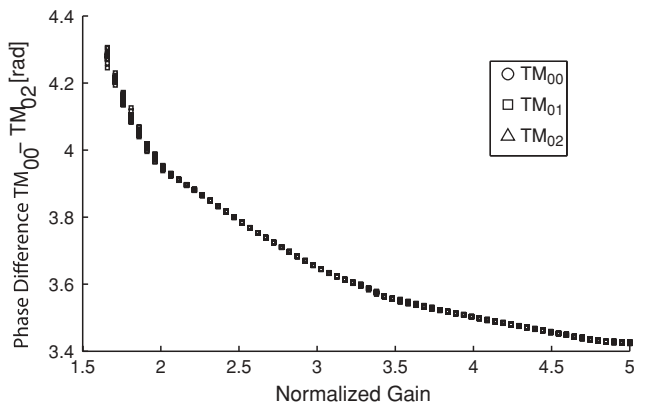

Fig. 7 Phases of the modes as a function of gain, normalized to g_{th}. The phase relation between the modes is a function of gain, resulting in beam steering of the field.

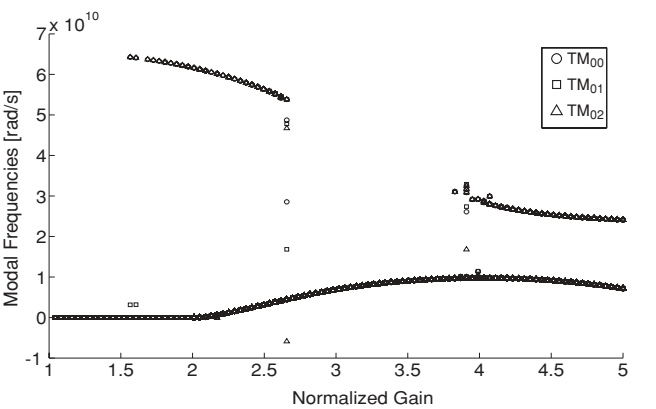

Fig. 9 Frequencies of all three modes locked to two different frequencies, normalized to g_{th}.

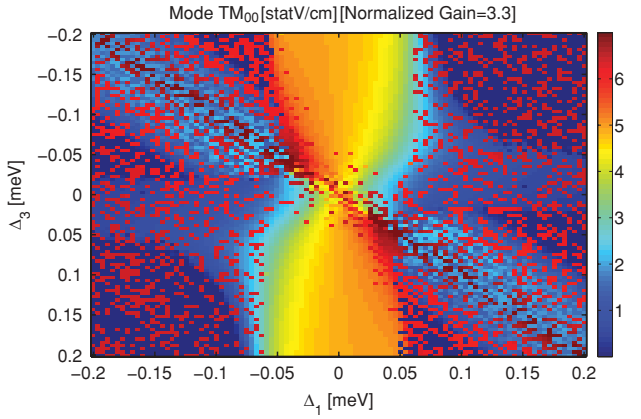

Fig. 10 The amplitudes of mode TM_{00} as a function of Δ.

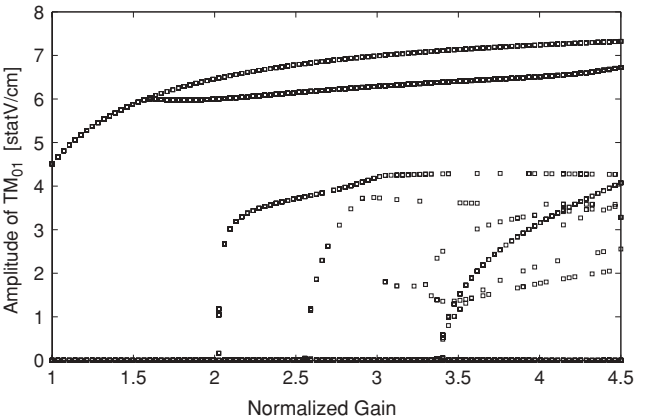

Fig. 12 Steady-state solutions as a function of gain for the mode TM_{01}.

detailed experimental study of the spectral distribution of the cavity modes has been performed by Stelmakh *et al.*[13] He found a broad range of values for spectral separation between lateral modes, from nearly degenerate cases of merging lateral modes to fairly large separations of the order of the distance between neighboring longitudinal modes (about 0.1 meV for a 2-mm-long cavity). Spectral position of cold cavity modes is an important design and optimization parameter for the control of nonlinear transverse mode dynamics.

The stable steady-state solutions found with the time-dependent analysis can be compared with a set of *all* frequency- and phase-locked steady-state solutions that can be obtained by eliminating time derivatives from the equations and solving for only the steady-state solutions. By changing the complex field variables into phases and amplitudes, we look for constant-amplitude, steady-state solutions of the form

$$a_j(t) = f_j \exp(i\Omega t + i\phi_j). \tag{13}$$

The amplitudes and phases f_j and ϕ_j become time independent and the modes lock to a single frequency Ω. The system of equations has one more unknown than the resulting number of equations. In this case it is possible to set one of the phases $\phi_j = 0$, without loss of generality, and eliminate one of the variables. The steady-state system of equations takes the following form,

$$\kappa_j f_j - g\Gamma_j f_j = \frac{-2g}{Is} \sum_{k,l,m} G_{jklm} f_k f_l f_m \cos\phi_{jklm},$$

$$\Omega f_j + \Delta_j f_j = \frac{-2g}{Is} \sum_{k,l,m} G_{jklm} f_k f_l f_m \sin\phi_{jklm},$$

$$\phi_{jklm} = \phi_k + \phi_l - \phi_m - \phi_j. \tag{14}$$

In our case, we take $\phi_2 = 0$. The solutions for the TM_{01} mode are presented in Fig. 12.

Both stable solutions from the bistability regime are present among all steady-state solutions. The change from the bistable to stable regime is accompanied by a change in the total number of steady-state solutions.

3.3 *Nonlinear Interactions of Cold Cavity Modes*

Now we make an assumption that is in a sense opposite to the mean-field approximation adopted before. We assume that the longitudinal dependence of the electric field corresponds to the standing wave modes in a cold lossless cavity, $\propto \sin(N_i \pi z/L_c)$, where L_c is the cavity length and N_i is an integer number of the order of 1800 for our lasers. This approximation neglects any z-dependence of modal amplitudes and carrier diffusion along z. The equations for the complex amplitudes Eq. (7) remain of the same form, only the modal index i becomes a double index, counting both transverse and longitudinal modes. Also, the overlap integrals G_{ijkl} now have to be taken over the cavity volume. These integrals contain the product of four sines with different arguments, so they are nonzero only for certain values of the longitudinal indices N_i.

One example of the spectral location of frequencies of cold cavity modes is schematically shown in Fig. 13(a). The spectrum can be split into triplets where each triplet consists of longitudinal modes that belong to different lateral modes and have different longitudinal indices. The separation between the modes within each triplet is determined by the geometry of the cavity. Various cases of mode alignment were explored with the spectrally resolved near-field measurements in Ref. 13. The lateral modes interact most efficiently when the overlap integral corresponding to the four-wave mixing process within each triplet is nonzero. Even in this case,

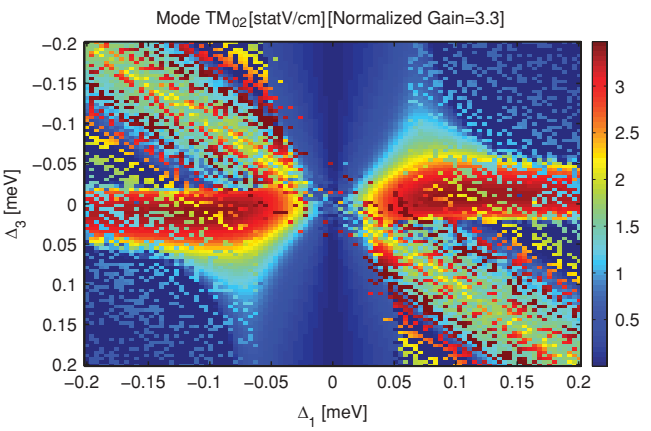

Fig. 11 The amplitudes of mode TM_{02} as a function of Δ.

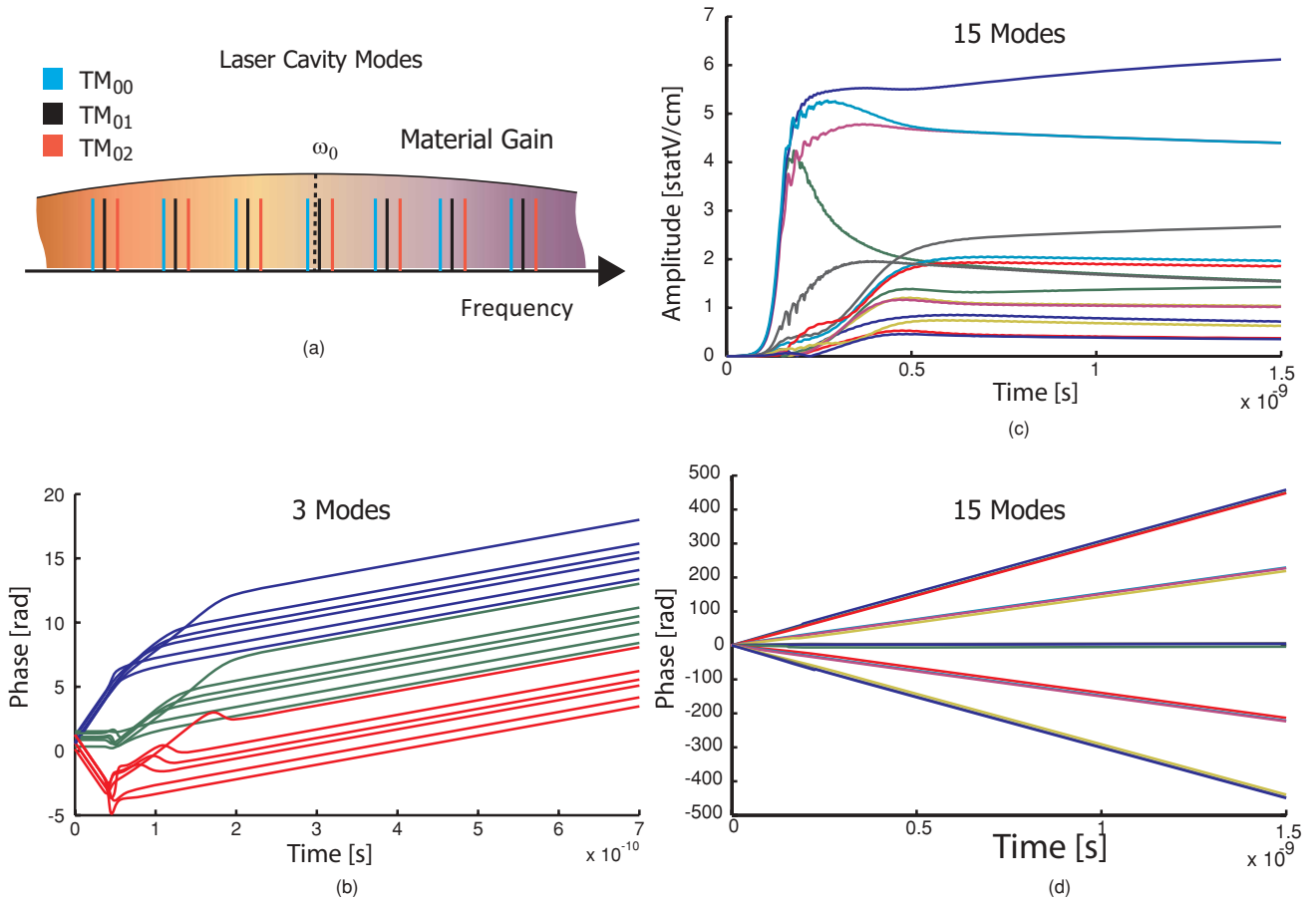

Fig. 13 Time-dependent simulations of frequency and phase locking between lateral combs at the current three times the threshold current. (a) Schematic of spectral positions of cold cavity modes. (b) Total phase of three modes constituting one triplet for six different initial conditions. (c) Amplitudes and (d) phases of all 15 modes for one initial condition.

the interaction is weaker than in the case of the mean-field approximation, because many interaction paths between the modes become forbidden. Nevertheless, simulations show that frequency and phase coupling are still possible.

Figures 13(b), 13(c), and 13(d) show the result of solving Eq. (7) when each of the three lateral modes consists of five longitudinal modes, resulting in five triplets. The separation of the modes within each triplet is about two times smaller than the distance $\hbar c\pi/(n_{eff}L_c) \sim 0.1$ meV between neighboring longitudinal modes. In Fig. 13(b), the dynamics of the total phases $\Theta_j(t)$ $\{a_j \propto \exp[i\Theta_j(t)]\}$ of three modes in a single triplet are shown for six randomly chosen initial con-

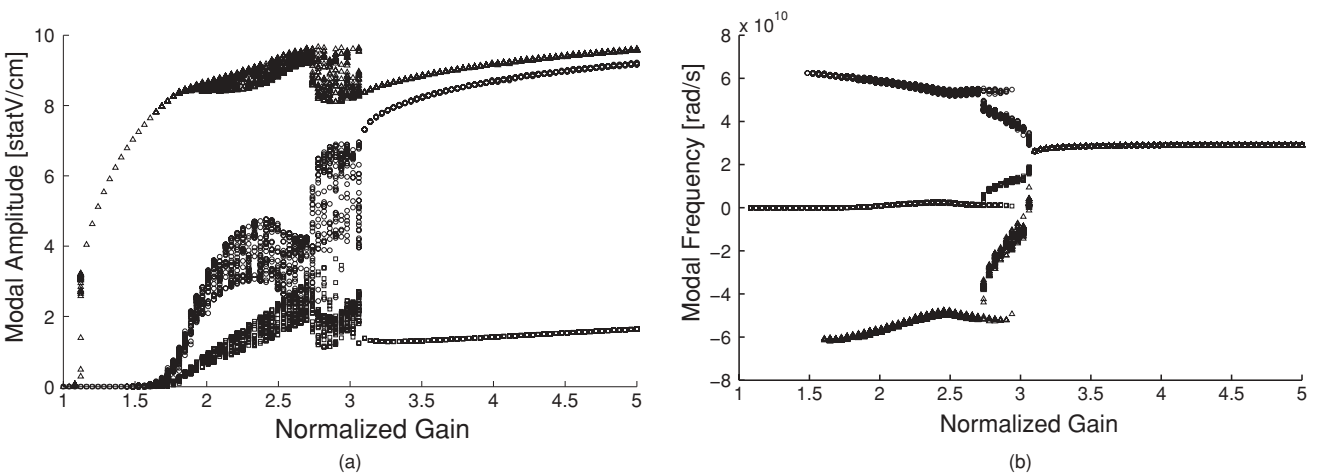

Fig. 14 Stable steady-state solutions for a large set of random initial conditions as the function of the linear gain normalized to the threshold gain for the TM_{02} mode. (a) Modal amplitudes and (b) modal frequencies.

ditions. Each mode is started from a random amplitude and phase. After the initial time of the order of the inverse growth rate of laser oscillations, frequencies of all three modes become locked to a single frequency independently on the initial conditions. Figure 13(d) demonstrates similar behavior for all five triplets. Moreover, we found that the evolution of modes constituting a single triplet is practically the same no matter how many triplets we included in the modeling. This allows us to consider in detail the dynamics of only one triplet.

Figure 14 shows the amplitude and frequencies of all *stable* steady-state solutions of Eq. (7) based on a large set of random initial conditions. For a given gain, we solve Eq. (7) starting from a set of random initial conditions and identifying the steady states that were asymptotically approached by time-dependent solutions. The frequency of each mode in Fig. 14 is defined as a derivative of the total phase; it is constant when the steady state is reached.

Simulations in Fig. 14 reveal the existence of a certain critical current above which there is only one stable steady-state solution. A remarkable feature of this solution is that frequencies of all modes are locked to the same frequency. Below this critical current, there are multiple steady-state solutions with different uncorrelated frequencies and phases.

4 Conclusions

In conclusion, we observe and theoretically analyze the effect of frequency and phase locking between lateral modes in buried-heterostructure QCLs. The effect persists for lasers of different designs and manufacturers over a broad range of injection currents. Therefore, transverse mode locking appears to be a universal phenomenon for high power QCLs that support multiple low-loss lateral modes.

Our data can be explained by phase-sensitive nonlinear coupling of transverse modes through resonant four-wave mixing interaction, mediated by inhomogeneous saturation of the active region (spatial hole burning). A model for the nonlinear dynamics of transverse modes in QCLs is derived and solved numerically. The numerical analysis predicts stable mode locking of multiple lateral modes. We find that nonlinear frequency pulling can lead to a complete synchronization of lateral modes: above a certain critical value of the injection current, the combs belonging to different lateral modes lock to a single comb with stable phase differences between lateral modes. This prediction is confirmed by observations.

For a low level of the amplitude and phase fluctuations, there may exist more than one stable phase-locked state. This multistability regime manifests itself by the presence of several separate combs in time-averaged measurements or as large intensity, fluctuations in the beam direction, and spectral fluctuations in time-resolved data.

The phase coupling of transverse modes can be affected and controlled by selectively inhomogeneous current injection, or by selective modulation of modal losses through the fabrication of metallic structures on top of the laser waveguide. The resulting frequency- and phase-locked multimode spectrum can be further utilized for creating stable midinfrared frequency combs and various far-field radiation patterns, controlling the beam quality and beam steering, or facilitating ultrashort pulse generation.

Acknowledgments

This work was supported in part by NSF grants ECS-0547019 (CAREER), EEC-0540832 (MIRTHE ERC), and ECCS-0925446.

References

1. N. Owschimikow, C. Gmachl, A. Belyanin, V. Kocharovsky, D. Sivco, R. Colombelli, F. Capasso, and A. Cho, "Resonant second-order nonlinear optical processes in quantum cascade lasers," *Phys. Rev. Lett.* **90**, 043902 (2003).
2. O. Malis, A. Belyanin, D. Sivco, J. Chen, A. Sergent, C. Gmachl, and A. Cho, "Milliwatt second-harmonic generation in quantum cascade lasers with modal phase-matching," *Electron. Lett.* **40**, 1586 (2004).
3. T. Mosely, A. Belyanin, C. Gmachl, D. Sivco, M. Peabody, and A. Cho, "Third harmonic generation in a quantum cascade laser with monolithically integrated resonant optical nonlinearity," *Opt. Express* **12**, 2972–2976 (2004).
4. M. A. Belkin, F. Capasso, A. Belyanin, D. L. Sivco, A. Y. Cho, D. C. Oakley, C. J. Vineis, and G. W. Turner, "Terahertz quantum-cascade-laser source based on intracavity difference frequency generation," *Nature Photon.* **1**, 288–292 (2007).
5. M. Belkin, F. Capasso, F. Xie, A. Belyanin, M. Fischer, A. Wittman, and J. Faist, "Room temperature terahertz quantum cascade laser source based on intracavity difference-frequency generation," *Appl. Phys. Lett.* **92**, 201101 (2008).
6. M. Troccoli, S. Corzine, D. Bour, J. Zhu, O. Assayag, L. Diehl, B. Lee, G. Hoer, and F. Capasso, "Room temperature continuous-wave operation of quantum-cascade lasers grown by metal organic vapour phase epitaxy," *Electron. Lett.* **41**(19), 1059–60 (2005).
7. Y. Khanin, *Principles of Laser Dynamics*, Elsevier, Amsterdam (1995).
8. C. Wang, L. Diehl, A. Gordon, C. Jirauschek, F. Kartner, A. Belyanin, D. Bour, S. Corzine, G. Hofler, M. Troccoli, J. Faist, and F. Capasso, "Coherent instabilities in a semiconductor laser with fast gain recovery," *Phys. Rev. A Rapid Commun.* **75**, 031802 (2007).
9. A. Gordon, C. Wang, L. Diehl, F. Kartner, A. Belyanin, D. Bour, S. Corzine, G. Hofler, H. C. Liu, H. Schneider, T. Maier, M. Troccoli, J. Faist, and F. Capasso, "Multimode regimes in quantum cascade lasers: From coherent instabilities to spatial hole burning," *Phys. Rev. A* **77**, 053804 (2008).
10. C. R. Menyuk and M. A. Talukder, "Self-induced transparency modelocking of quantum cascade lasers," *Phys. Rev. Lett.* **102**, 023903 (2009).
11. C. Y. Wang, L. Kuznetsova, V. M. Gkortsas, L. Diehl, F. X. Kärtner, M. A. Belkin, A. Belyanin, X. Li, D. Ham, H. Schneider, P. Grant, C. Y. Song, S. Haffouz, Z. R. Wasilewski, H. Liu, and F. Capasso, "Mode-locked pulses from mid-infrared quantum cascade lasers," *Opt. Express* **17**, 12929–12943 (2009).
12. N. Yu, L. Diehl, E. Cubukcu, D. Bour, S. Corzine, J. Zhu, G. Höfler, A. Wójcik, K. Crozier, A. Belyanin, and F. Capasso, "Coherent coupling of multiple transverse modes in quantum cascade lasers," *Phys. Rev. Lett.* **102**, 013901 (2009); A. K. Wójcik, N. Yu, L. Diehl, F. Capasso, and A. Belyanin, "Self-synchronization of laser modes and multistability in quantum cascade lasers," *Phys. Rev. Lett.*, submitted.
13. N. Stelmakh, M. Vasilyev, F. Toor, and C. Gmachl, "Degenerate and nondegenerate lateralmode patterns in quantum cascade lasers," *Appl. Phys. Lett.* **94**, 013501 (2009).
14. L. A. Lugiato, F. Prati, L. M. Narducci, P. Ru, J. R. Tredicce, and D. K. Bandy, "Role of transverse effects in laser instabilities," *Phys. Rev. A* **37**(10), 3847–3866 (1988).
15. W. Kaige, N. B. Abraham, and L. A. Lugiato, "Leading role of optical phase instabilities in the formation of certain laser transverse patterns," *Phys. Rev. A* **47**(2), 1263–1273 (1993).
16. D. L. Andrews, *Structured Light and its Applications: An Introduction to Phase-Structured Beams and Nanoscale Optical Forces*, Academic Press, Amsterdam (2008).
17. M. Brambilla, M. Cattaneo, L. A. Lugiato, R. Pirovano, F. Prati, A. J. Kent, G.-L. Oppo, A. B. Coates, C. O. Weiss, C. Green, E. J. D'Angelo, and J. R. Tredicce, "Dynamical transverse laser patterns. i. theory," *Phys. Rev. A* **49**(2), 1427–1451 (1994).
18. C. Denz, P. Jander, M. Schwab, O. Sandfuchs, M. Belić, and F. Kaiser, "Transverse pattern formation and its control in photorefractive optics," *Ann. Phys.* **13**(7-8), 391–402 (2004).
19. P. Mandel and M. Tlidi, "Transverse dynamics in cavity nonlinear optics (2000-2003)," *J. Opt. B: Quantum Semiclass. Opt.* **6**(9), R60 (2004).
20. N. B. Abraham and W. J. Firth, "Overview of transverse effects in nonlinear-optical systems," *J. Opt. Soc. Am. B* **7**(6), 951–962 (1990).
21. W. Bewley, J. Lindle, C. S. Kim, I. Vurgaftman, J. Meyer, A. Evans, J. S. Yu, S. Slivken, and M. Razeghi, "Beam steering in high-power cw quantum-cascade lasers," *IEEE J. Quantum Electron.* **41**(6), 833–841 (2005).
22. B. Hinkov, F. Fuchs, W. Bronner, K. Kohler, and J. Wagner, "Current- and temperatureinduced beam steering in 7.8 μm- emitting

quantum-cascade lasers," *IEEE J. Quantum Electron.* **44**(11), 1124–1128 (2008).
23. N. Yu, R. Blanchard, J. Fan, Q. J. Wang, C. Pflugl, L. Diehl, T. Edamura, S. Furuta, M. Yamanishi, H. Kan, and F. Capasso, "Plasmonics for laser beam shaping," *IEEE Trans. Nanotechnol.* **9**(1), 11–29 (2010).
24. R. Lang, "Lateral transverse mode instability and its stabilization in stripe geometry injection lasers," *IEEE J. Quantum Electron.* **QE-15**, 718–726 (1979).
25. Q. J. Wang, C. Pflugl, L. Diehl, F. Capasso, T. Edamura, S. Furuta, M. Yamanishi, and H. Kan, "High performance quantum cascade lasers based on three-phonon-resonance design," *Appl. Phys. Lett.* **94**(1), 011103 (2009).
26. L. Diehl, D. Bour, S. Corzine, J. Zhu, G. Hofler, M. Loncar, M. Troccoli, and F. Capasso, "High-power quantum cascade lasers grown by low-pressure metal organic vapor-phase epitaxy operating in continuous wave above 400 K," *Appl. Phys. Lett.* **88**(20), 201115 (2006).
27. F. Rana and R. J. Ram, "Current noise and photon noise in quantum cascade lasers," *Phys. Rev. B* **65**(12), 125313 (2002).
28. T. Gensty, W. Elsäßer, and C. Mann, "Intensity noise properties of quantum cascade lasers," *Opt. Express* **13**(6), 2032–2039 (2005).
29. N. Yu, L. Diehl, E. Cubukcu, C. Pögl, D. Bour, S. Corzine, J. Zhu, G. Höfler, K. B. Crozier, and F. Capasso, "Near-field imaging of quantum cascade laser transverse modes," *Opt. Express* **15**(20), 13227–235 (2007).

Biographies and photographs of the authors not available.